Chapter 5

Dry High Speed Orthogonal Turning of Titanium Alloy Wear Evolution and Chip Morphology

Mohieddine Benghersallah, Lakhdar Boulanouar, Gautier List and Guy Sutter

Additional information is available at the end of the chapter

http://dx.doi.org/10.5772/intechopen.78669

Abstract

The present work is an experimental study on the dry high-speed turning of Ti-6Al-4 V titanium alloy. The objective of this study is to see for high cutting speeds, how wear occurs on the face of insert and how to evolve cutting forces and chip formation. Cutting speeds tested is 600, 800, 1000 and 1200 m/min in orthogonal turning with a carbide insert tool H13A uncoated and coated TiN on a cylindrical titanium alloy part. Investigation on the wear inserts with 3D microscope scanning revered the crater formation is instantaneous and a chip adhesion. Welded chip causes detachment of carbide particles. In these experiments the chip shape was systematically investigated at each cutting conditions using optical microscopy. The chips produced were collected and polished to measure the thicknesses t_{2max} and t_{2min}. The distance between each segments d_{ch} and ϕseg inclination angle as described in the introduction part, the shear angle ϕ and the inclination angle of a segment ϕseg are differentiated. ϕseg angle is actually measured on the collected chips while the shear angle ϕ cannot be. The angle ϕ represents the initial shear similar to the one that describes the formation of a continuous chip in the primary shear zone. Cutting forces increase and stabilize before removing the tool. The chip reaches a very high temperature.

Keywords: titanium alloys, dry high-speed machining, chip formation, cutting zone, confocal imaging

1. Introduction

Titanium alloys such as Ti–6Al–4 V, Ti-555, Ti6242S, and Ti-LCB, are used extensively in the aerospace industry for structural components (compressor blades, disks, castings, and gas

turbine engines) due to their superior properties such as excellent strength-to-weight ratio, strong corrosion resistance and ability to retain high strength at high temperatures [1–3]. Light-weight materials such as titanium alloys are now used in modern aerospace structure due to their best combination of metallurgical and physical properties. Each class of titanium alloy has their advantages and disadvantages. Titanium's advantages are high strength-to-weight ratio, low density, excellent corrosion resistance, excellent erosion resistance and low modulus of elasticity.

Ti-6Al-4 V may be considered in any application where a combination of high strength at low to moderate temperatures, light weight and excellent corrosion resistance are required. Some of the many applications where this alloy has been used include aircraft turbine engine components, aircraft structural components, aerospace fasteners; high-performance automotive parts, marine applications, medical devices, and sports equipment [1–4].

Titanium and its alloy have poor machinability, this may be due to their high chemical reactivity with most cutting tools and therefore, have a tendency to weld to the cutting tool during machining, thus leading to chipping and premature tool failure. Its low thermal conductivity increases the temperature at the tool/work piece interface, which affects the tool life [2, 3, 5].

Minimum quantity lubrication (MQL) is widely applied for titanium alloy machining, meanwhile, in the machining process of titanium alloy, there are several problems regarding tool wear, poor surface damage, and machining deformation. Moreover, surface damage usually appears during high-speed machining. Therefore, the contradiction between increasing machining demand and machining performance has become a bottleneck in actual industry.

On the other hand, there are critical needs to reduce the usage of cutting fluid in machining process in order to reduce the environmental burden and economic cost [3]. Dry and minimum quantity lubrication (MQL) machining which are two types of green manufacturing processes have vast potentials for machining of titanium alloys [4–6]. Additionally, the tool coating is a key factor to realize high-speed machining and green manufacturing. Coating materials is widely employed to extend tool life and cutting performance of cutting tools due to their advanced wear resistance and superior performance under corrosive or high temperature conditions. However, the tool coatings used presently in machining of titanium alloys cannot meet with the need of high-speed machining and green manufacturing. Simultaneously, as one of an effective green manufacturing technology, the combination of MQL and novel cutting tools is also growing.

1.1. Topographic tool wear characterization

In recent years, many microscopy techniques were commonly used for characterizing the surface topography in many scientific fields (**Figure 1**) [7, 14, 20].

The atomic force microscopy (AFM), stylus profilometry, stereo microscopy (SM), scanning electron microscopy (SEM), reflected light interference microscopy (RLIM), and confocal laser scanning microscopy (CLSM). The first two are touch instruments, while others are non-contact instruments. AFM, the state of the art profiler, has excellent depth and transverse resolution.

http://dx.doi.org/10.5772/intechopen.78669

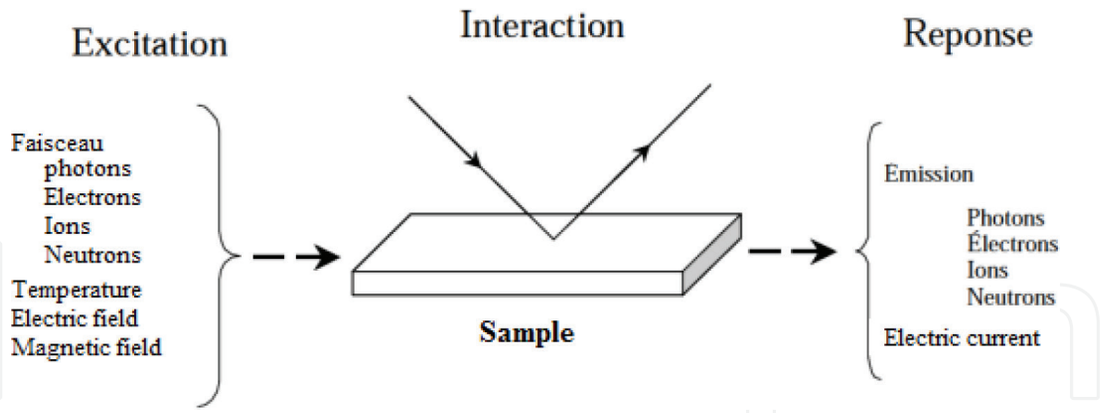

Figure 1. General principle of surface characterization methods [7].

However, its disadvantages such as slow scan very small field sample (usually 70 × 70 um), restricted depth range (about 5 μm), its inability to scan deep holes, and the extreme fragility of the tip prevented its immediate application to tool wear analysis [8–11].

In the conventional optical microscope, the image is "flat", providing lateral dimensional information (X and Y), but not axial (Z). The image contrast is derived generally in variations of surface reflectivity. Confocal microscopy provides quantitative information on the optical axis (Z). The principle of the confocal microscope is to focus, through a goal, a laser beam will illuminate a point of the sample, then recovering on a photomultiplier, the light signal emitted at this point [12, 13].

Confocal microscopy is a non-destructive optical technique to obtain optical sections not only in the plane (X, Y), but also along a plane (X, Z) parallel to the optical axis which can be obtained a three-dimensional reconstructions [14]. These optical sections "virtual" do not affect the entire sample unlike physical cuts necessary in electron microscopy. The latest developments in fluorescent confocal microscopy allow, for marking means based on the use of fluorescent products, observe remarkable 3D structures.

One of the drawbacks of confocal microscopy is its slow action. Indeed, the measurement of a 3D structure requires up to a few hours.

The principle of the operation of the confocal microscope is shown in **Figure 2**. Light emitted from the source after passing through the optical path is focused on the analyzed surface. The reflected beam reaches to a diaphragm which transmits only focused light and to a photodetector. A vertical scanning system is moving the lens, which allows to analyze different height areas of roughness. That ability to distinguish height improves significantly the contrast and the lateral resolution in comparison with the classic optical microscope. Scanning confocal microscopes took advantage of the differentiation of depth and generating of surface image and reception of reflected beam is done by the same optical system. Like in the scanning method, the optical system generates a spot on a surface, and a reflected light beam is recorded by a point detector. In the construction of a diaphragm of a modern confocal microscope a Nipkow disk with a series of spiral splitting small holes is used. In connection with a

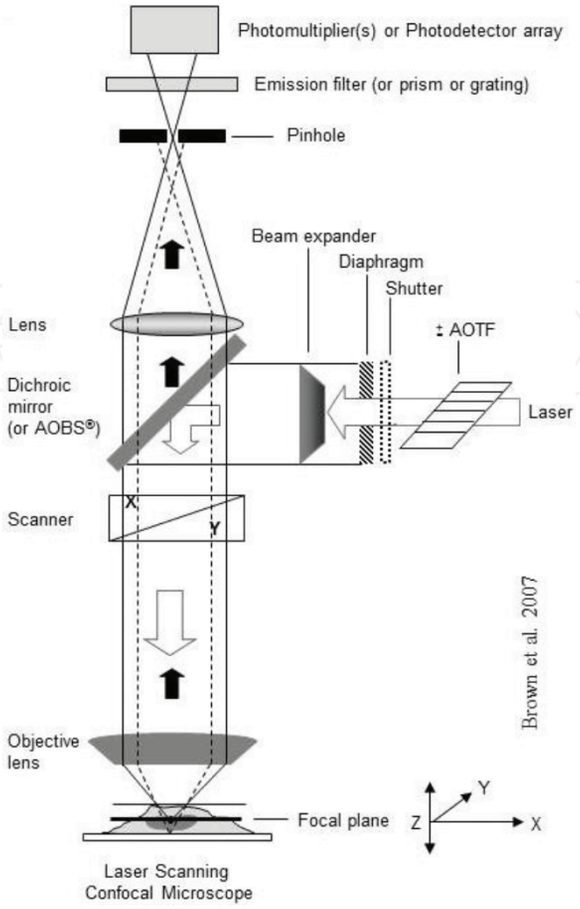

Figure 2. Confocal microscopic principle [7, 15–17].

suitably prepared light beam (after passing through another Nipkow disk with microlenses) it allows a scan of the surface topography effectively.

The scanning microscope in recent years has been generally accepted. It is a tested and approved technique on the nano scale, which allowed to obtain very good vertical resolution. Serious problems appear only in the case of very rough surfaces and the necessity to use a larger vertical range. Microscope application can cause a little difficulty in the interpretation of results of measurement, especially when samples have inclusions or impurities on the surface, which characteristics are variable or can have an influence on response of instrument [14].

The cutting edge shape and the cutting edge condition are of crucial importance for machining operations. During the cutting process the impact of high thermal and mechanical loads on the cutting edge result in wear. Moreover, the quality of the machined surface is affected by the cutting edge shape. The demands of modern production are high productivity and high process reliability. One place these demands can be met is in cutting edge preparation [13, 14, 18].

Tool wear is one of the most complex problems in machining because it is affected by various factors such as the behavior of the work material, the interaction of the work material with the cutting tool, machining condition, dynamics, and the stability of machining tools. This makes the identification of the dominating wear mechanisms very difficult. The development of wear models based on these wear mechanisms, the interfacial stress and temperature fields

determination, and the topography characterization of tool wear stand out among the most urgent issues in this area of research. If these issues can be resolved, tool life can be easily predicted and the effectiveness of cutting tools improved.

Tool life is dictated by catastrophic failure, plastic deformation, and gradual wear. The first two imply premature failures of a tool and, therefore, should be avoided at all times. Gradual wear is the main interest because it limits tool life in a typical machining condition. The most common forms of gradual tool wear are flank wear and crater wear. Flank wear limits the service life of a tool directly because it affects dimensional accuracy, forces generated, and power consumption. Crater wear can reduce the cutting forces. However, the weakening of the cutting edge ultimately leads to failure. Crater wear represents a greater challenge than flank wear due to many competing wear mechanisms, such as abrasion, dissolution, and/or diffusion [14, 18].

1.2. Tool wear mechanisms

For many years, the study of tool wear has been limited to empirical approaches. The well-known empirical Taylor's equation, for example, is convenient when dealing with few work materials and cutting tools. However, it is unable to predict the performance of new work and tool materials without a substantial amount of machining experiments. Therefore, such an empirical equation cannot be used in the development of new cutting tools. On the other hand, some researchers [13, 14, 19–24] have approached tool wear from physics-based models.

The main wear mechanisms involved in tool wear have been proposed to be adhesion, abrasion, diffusion, and dissolution. Flank wear is caused mainly by abrasion of the hard second phase in a work material. Crater wear is controlled by a combination of adhesion, abrasion, dissolution, and/or diffusion [15, 17, 25, 27, 29, 30]. At present, it is not clear exactly which mechanisms dominate crater wear in relation to the cutting condition. In high-speed machining, crater wear is believed to be dominated by dissolution wear and subsequent diffusion [15–17, 25–27]. The aim of this paper is to explain qualitatively the high crater wear resistance of multilayer coated carbides through the observation and analysis of their confocal topography.

2. Experimental work

The workpiece is a Ti–6Al–4 V alloy bar with a length of 300 mm and a diameter of 110 mm. **Tables 1** and **2** show the chemical composition and physical properties of the titanium alloy, respectively.

The machining trials were carried out on a CNC lathe, with a 22 kW motor drive with a maximum torque of 2000 Nm. The spindle rotation speed ranges from 18 to 4500 rpm.

All cutting tests were carried out with uncoated carbide inserts (H13A-P15, 6% Co and 94% WC) without chip-breaker, with a rake angle $\gamma = 0°$ and a clearance angle of 7° [21].

The cutting forces were measured at the early stages of machining up to 1 minute, when the inserts have not suffered appreciated wear, with a piezoelectric Kistler dynamometer (**model 9441B**), connected to a charge amplifier.

Al	V	Fe	O_2	H_2	N_2	Ti
6	4	0.03	0.01	0.01	0.25	Balance

Table 1. Nominal composition of Ti-6Al-4 V (wt.%).

Tensile strength (MPa)	0.2% Proof stress (MPa)	Density (g/cm^3)	Elongation 5D (%)
960 ± 1270	885	4.42	8
Reduction of area (%)	Modulus of elasticity tension (GPa)	Hardness (Hv)	Thermal conductivity (W/mK)
25	100–130	330–370	7

Table 2. Mechanical and thermal properties of Ti–6Al–4 V.

The tool inserts were used to machine the titanium alloy at the following conditions:

- Cutting speeds (m/min): 600, 800, 1000, 1200 m/min
- Feed rate (f): 0.1 mm/rev.
- Depth of cut: 3 mm

The test is to be machined orthogonally the workpiece on a depth ap = 0.3 mm and feed rate f = 0.1 mm/rev. with five cutting speed values according (600, 800, 1000, 1200 m/min) (**Figure 3**).

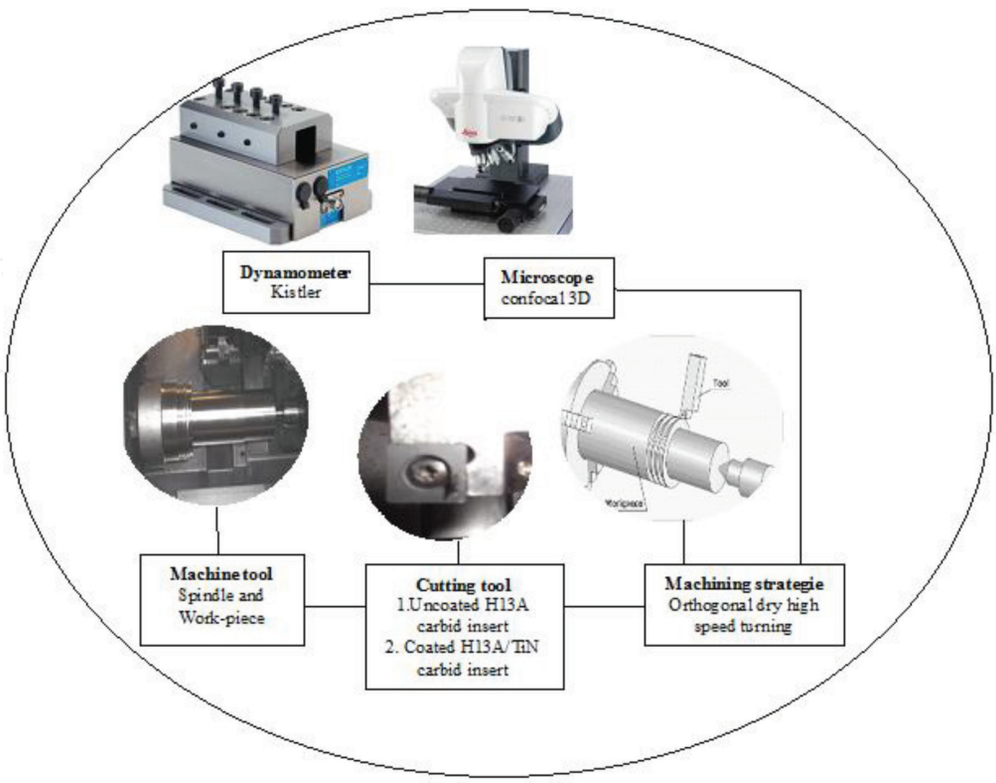

Figure 3. Schematic diagram of experimental setup.

http://dx.doi.org/10.5772/intechopen.78669

3. Results and discussion

A. Wear investigations

First investigations concerning the wear inserts to know if the H13A [28] tool material resists wear for very high cutting speeds.

The microscope photography shows a welding chip on the rake face. The temperature in the cutting zone reaches values near to the melting temperature of the material being machined. Instantly the chip stands and removed with him the substrate material of the tool which causes the crater wear.

Figure 4 shows the confocal image obtained by the microscope DCM3D of the cutting insert for the machining conditions (V c = 600 m/min, f = 0.1 mm, ap = 3 mm) on this picture we can see the welded chip on the rake face. **Figure 4c**), shows the profile diagram of the cutting insert obtained by skew right A. A on unworn cutting edge and the profile of crater obtained between welding chip zone by skew right B.B.

Figure 5a is a microscope photography of the cutting zone on the insert according the cutting parameters (800 m/min, f = 0.1 mm/rev, ap = 3 mm) on the rake face we can see the crater wear formation. **Figure 5b** shows 3D image of cutting insert according the cutting parameters, we can see the crater wear formation in rake face and collapse of cutting edge. **Figure 5c** shows the profile of crater wear obtained by skew right A.A.

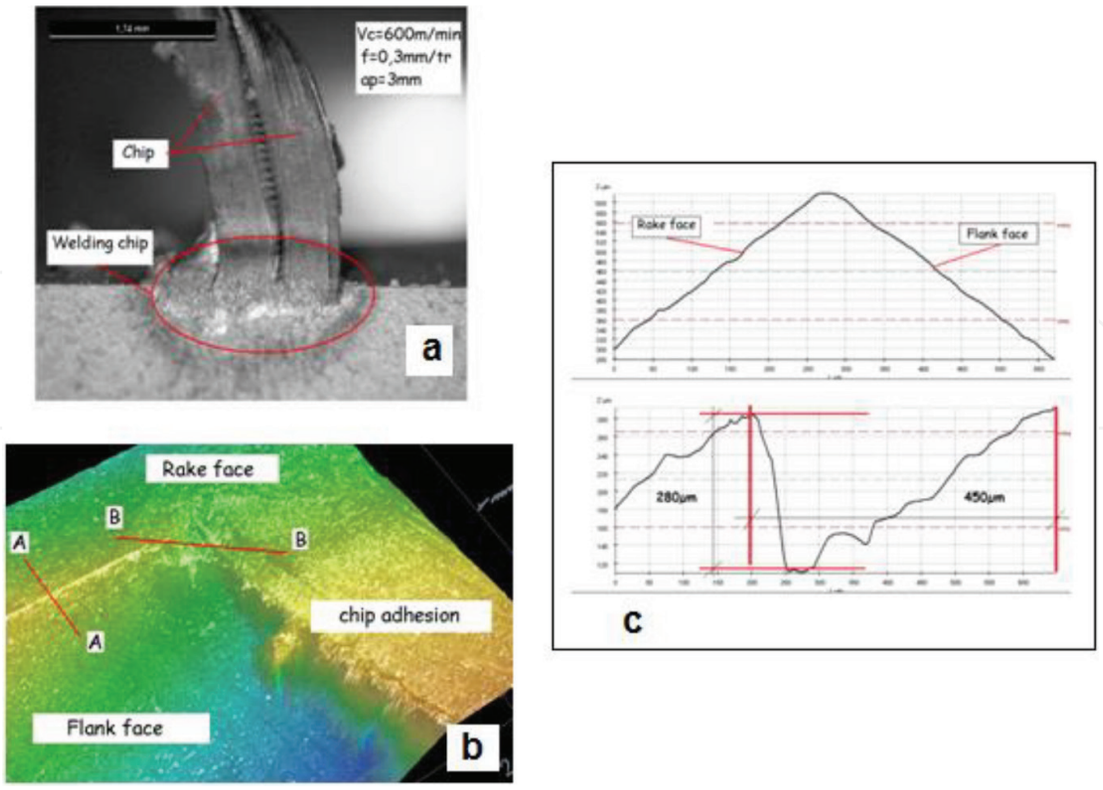

Figure 4. (a) Photography of chip welding on rake face, (b) 3D confocal image of the cutting insert (600 m/min, f = 0.1 mm/rev, ap = 3 mm), (c) profile diagram obtained by skew right unworn cutting edge and profile of crater failure under chip welding.

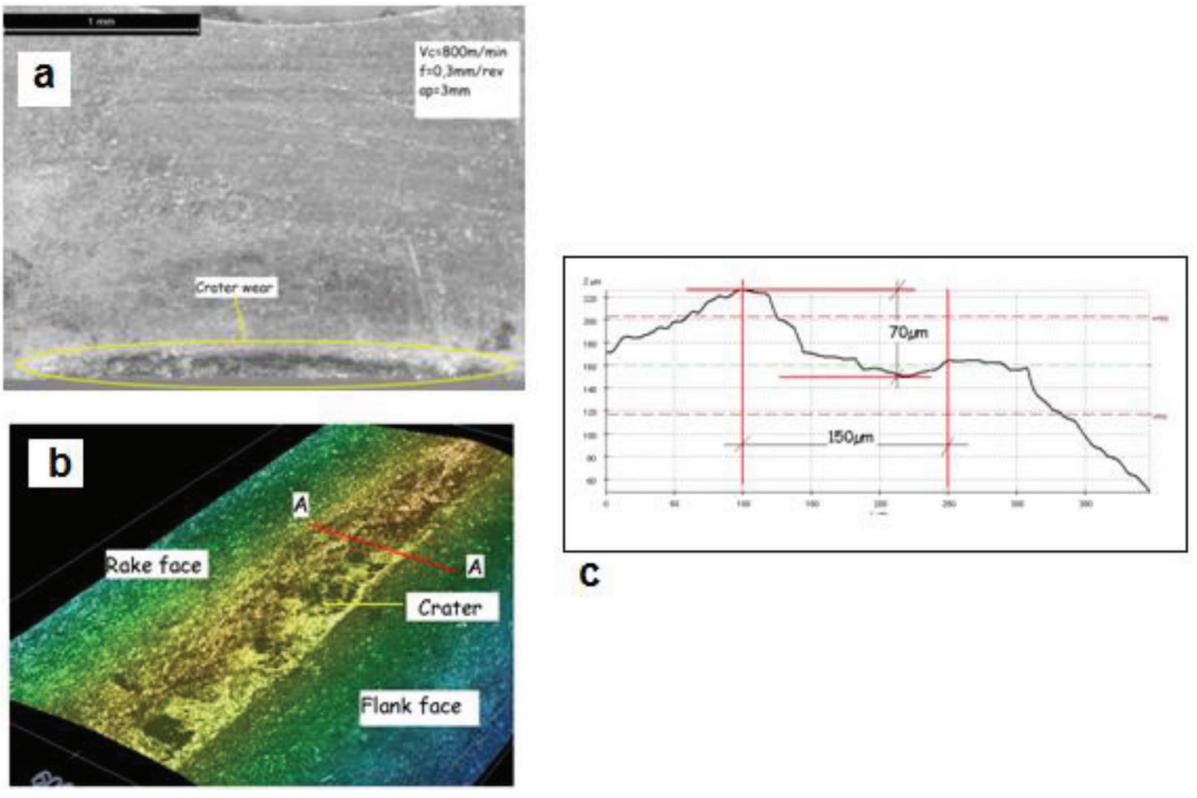

Figure 5. (a) Photography of cutting edge insert (b) 3D confocal image of the cutting insert according the cutting parameters (800 m/min, f = 0.1 mm/rev, ap = 3 mm), (c) crater profile by skew right A.A.

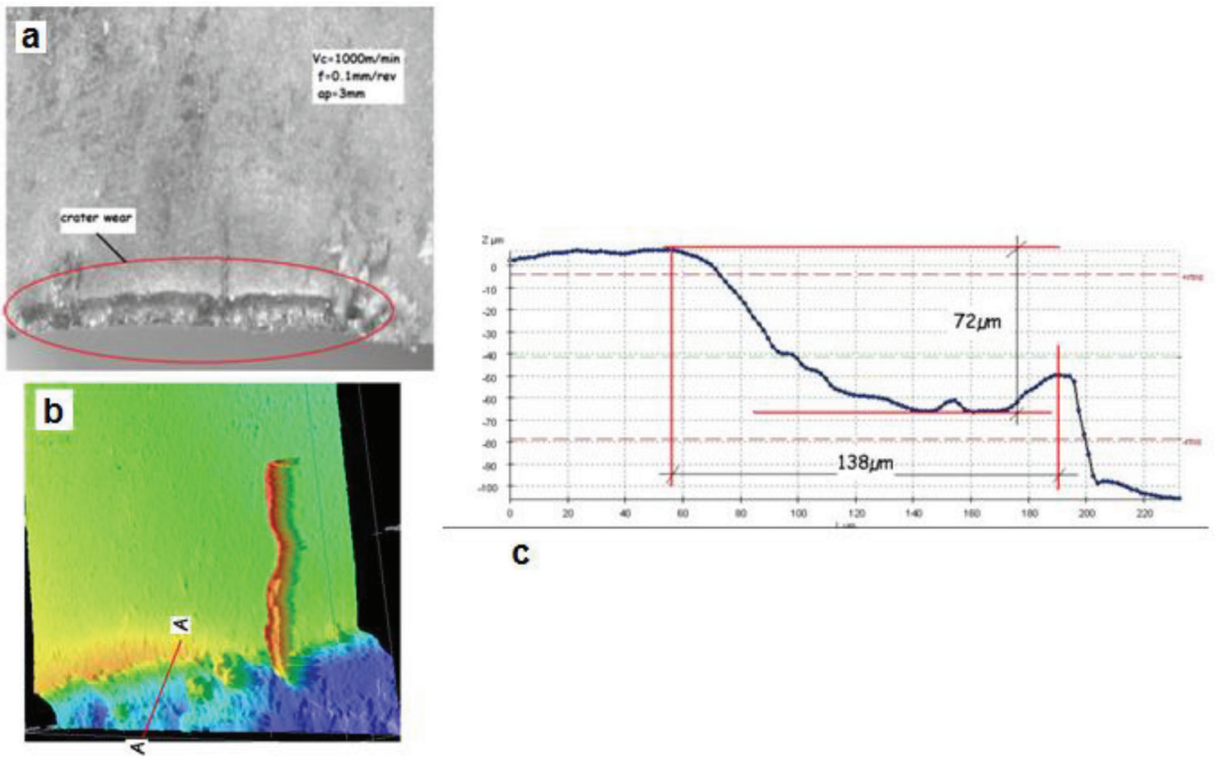

Figure 6. (a) Photography of cutting zone of insert according the cutting parameters (1000 m/min, f = 0.1 mm/rev, ap = 3 mm), (b) 3D confocal image, (c) profile 2D of crater wear.

http://dx.doi.org/10.5772/intechopen.78669

The photography of optical microscope (**Figure 6a**) show the insert according the cutting parameters (Vc = 1000 m/min, f = 0.1 mm/rev, ap = 3 mm). We can see the crater wear and chip adhesion in different area. **Figure 6b** show in 3D image confocal the chip welded and crater wear and the collapse at the sharp ridge. In **Figure 6c**, the crater wear values are defined with the 2D profile.

The photography of optical microscope (**Figure 7a**) show the insert according the cutting parameters (Vc = 1200 m/min, f = 0.1 mm/rev, ap = 3 mm). We can see the crater wear formation on rake face. **Figure 7b**, show in 3D image confocal the crater wear and the collapse at the sharp ridge. In **Figure 7c**, the crater wear values are defined with the 2D profile.

Early investigations clearly show that for very high cutting speeds, the plate wears quickly. This is due to excessive heating of the cutting area. The temperature in the cutting zone reaches superior to the melting temperature of Ti-6Al-4 V values. This material known for its poor thermal conductivity welds.

3.1. Confocal imaging of coated TiN insert

The confocal image of the **Figure 8a** shows a portion of the H13A TiN coating insert during the cutting parameters (Vc = 600 m / min, f = 0.1 mm / rev, ap = 3 mm). On the flank face we observed a welding chip of Ti6Al4V titanium alloy. The temperature in the cutting zone is very high, the chip is welded, it causes wear in crater on the rake face. This crater is born after the posting of the substrate particles forming the insert. The predominant wear is by adhesion. The confocal image of the **Figure 8b** shows the wear on the H13A TiN coating insert

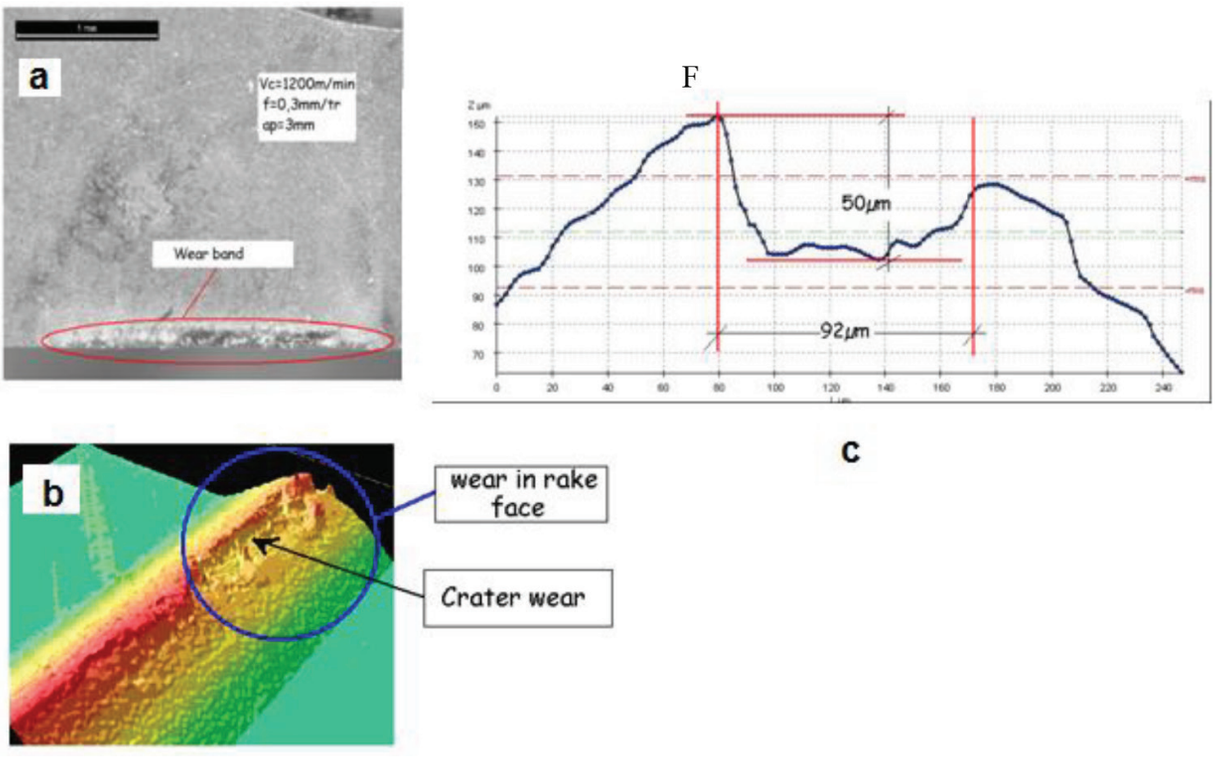

Figure 7. (a) Photography of cutting edge according (Vc = 1200 m/min, f = 0.1 mm/rev, ap = 3 mm). (b) 3Dconfocal image, (c) profile 2D of crater wear.

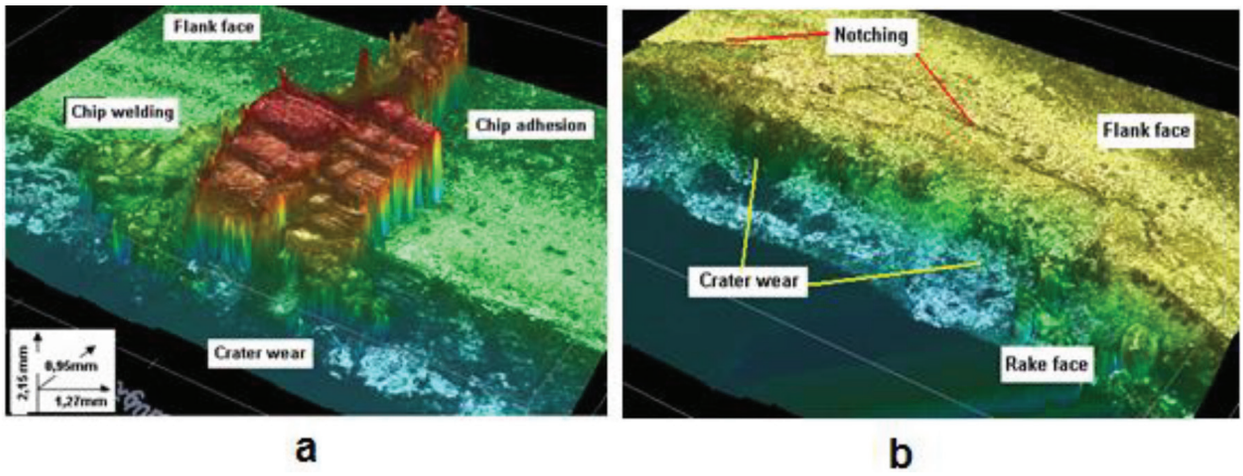

Figure 8. (a) 3D confocal image according (600 m/min, f = 0.1 mm/rev, ap = 3 mm) for coating TiN insert, (b) 3D confocal image according (Vc = 800 m/min, f = 0.1 mm/rev, ap = 3 mm) for coating TiN insert.

for the cutting parameters (Vc = 800 m/min, f = 0.1 mm/rev, ap = 3 mm). On the rake face we observed the crater wear formation caused by the adhesion of the titanium alloy chip. The chip is welded and then migrates under the high-speed action of next chip. On the rake face coating stands served and the increase in flank wear by abrasion to the total damage of the cutting edge.

The confocal image of the **Figure 9a** shows the wear on the insert for the cutting speed (Vc = 1000 m/min, f = 0.1 mm/rev, ap = 3 mm). The particles of the welding chip are observed. Tearing of these chips causes a crater by wear adhesion. The chip welded titanium migrate under the effect of the high-speed thrust next chip. On the flank face we observed the formation of the band of the flank wear and the effect of the temperature with the detachment of the coating. The confocal image of the **Figure 9b** shows the wear on the coating insert for the cutting parameters (Vc = 1200 m /min, f = 0.1 mm/rev, ap = 3 mm). On the rake face there is a

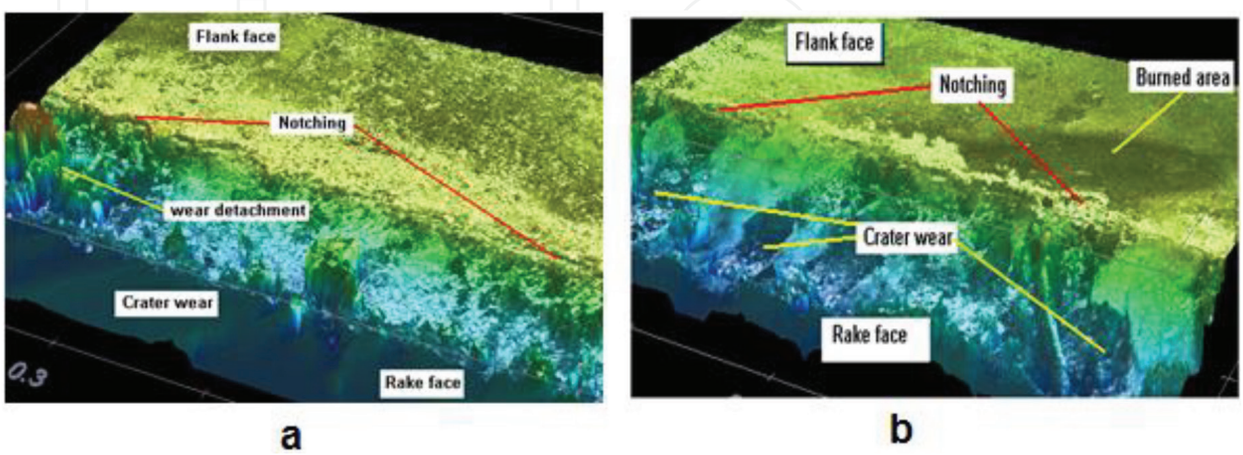

Figure 9. (a) 3D confocal image according (Vc = 1000 m/min, f = 0.1 mm/rev, ap = 3 mm) for coating TiN insert, (b) 3D confocal image according (Vc = 1200 m/min, f = 0.1 mm/rev, ap = 3 mm) for coating TiN insert.

very pronounced crater wear caused by tearing of the chip that forces the particles from the substrate to detach. The next chip and forms a crater wear. On the flank face we observed the formation of the band of the flank wear and the effect of the temperature of the chip in combustion phase leaving burn marks.

The overall analysis of 3D confocal images shows that the dominant wear for orthogonal turning high-speed titanium is the main crater wear caused by adhesion.

3.2. 2D profiles of crater wear measurements

Figure 10 shows the profiles of the craters of each insert under different cutting conditions, we can give the depth of each crater.

3.3. Diagram of crater wear evolution

Figure 11 shows the evolution of the depth of rake face crater for different parameters of cutting regime and for the two types of inserts. With uncoated insert the largest depth of the crater is recorded for 600 m/min testing. The depth of KT has decreased for 800 m/min cutting speed, it increases significantly for 1000 m/min. At 1200 m/min we noticed a sharp decrease in crater depth. For TiN coated insert, the value of the crater depth is substantially the same. This is due to the coating which is a barrier against crater wear.

B. Flank wear characterization

In **Figure 12** confocal image is observed from the flank face of the H13A TiN coating insert following conditions:

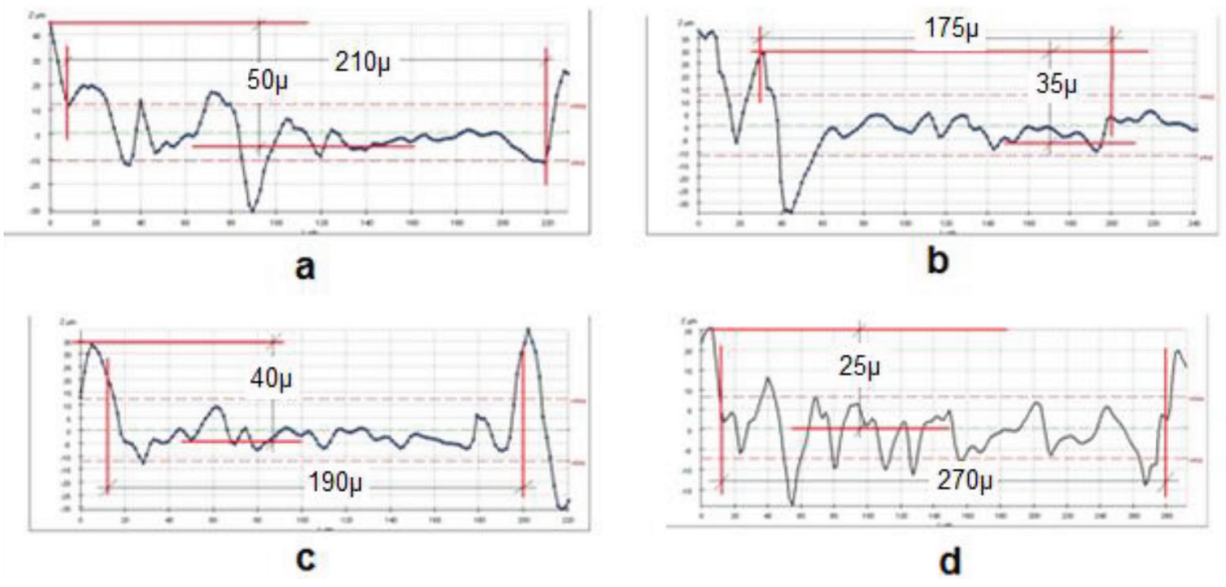

Figure 10. (a) 2D profile of crater wear according the following conditions (Vc = 600 m/min, f = 0.1 mm/tr, ap = 3 mm). (b) 2D profile of crater wear according the following conditions (Vc = 800 m/min, f = 0.1 mm/tr, ap = 3 mm). (c) 2D profile of crater wear according the following conditions (Vc = 1000 m/min, f = 0.1 mm/tr, ap = 3 mm). (d) 2D profile of crater wear according the following conditions (Vc = 1200 m/min, f = 0.1 mm/tr, ap = 3 mm).

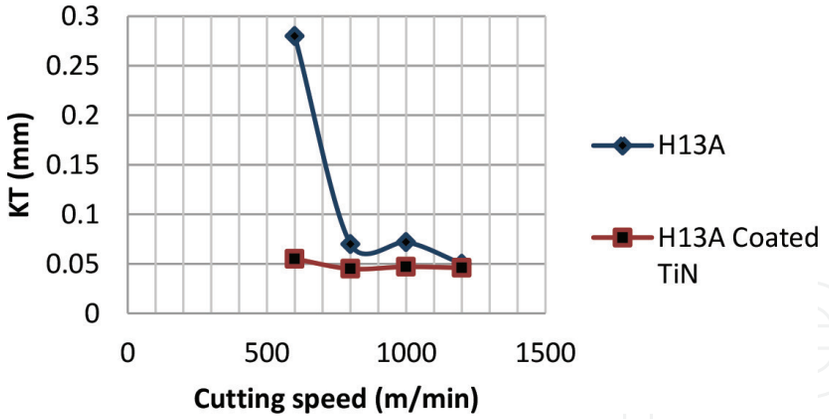

Figure 11. Crater wear evolution for two carbides inserts according the cutting parameters.

(a) (Vc = 600 m/min, f = 0.1 mm/rev, ap = 3 mm). Wear is caused by the friction of the workpiece on the flank face, the predominant wear is obtained under the effect of abrasion accompanied by the wear caused by the migration of the substrate particles removed by the adherent chip. **Figure 12b** shows for the conditions (Vc = 800 m/min, f = 0.1 mm/rev, ap = 3 mm), the chip welding on the rake face has been abraded by rubbing on the workpiece surface. The chip detachment will generate a catastrophic wear caused by the detachment of the substrate. **Figure 9c** shows the conditions (Vc = 1000 m/min, f = 0.1 mm/rev, ap = 3 mm), we observe a

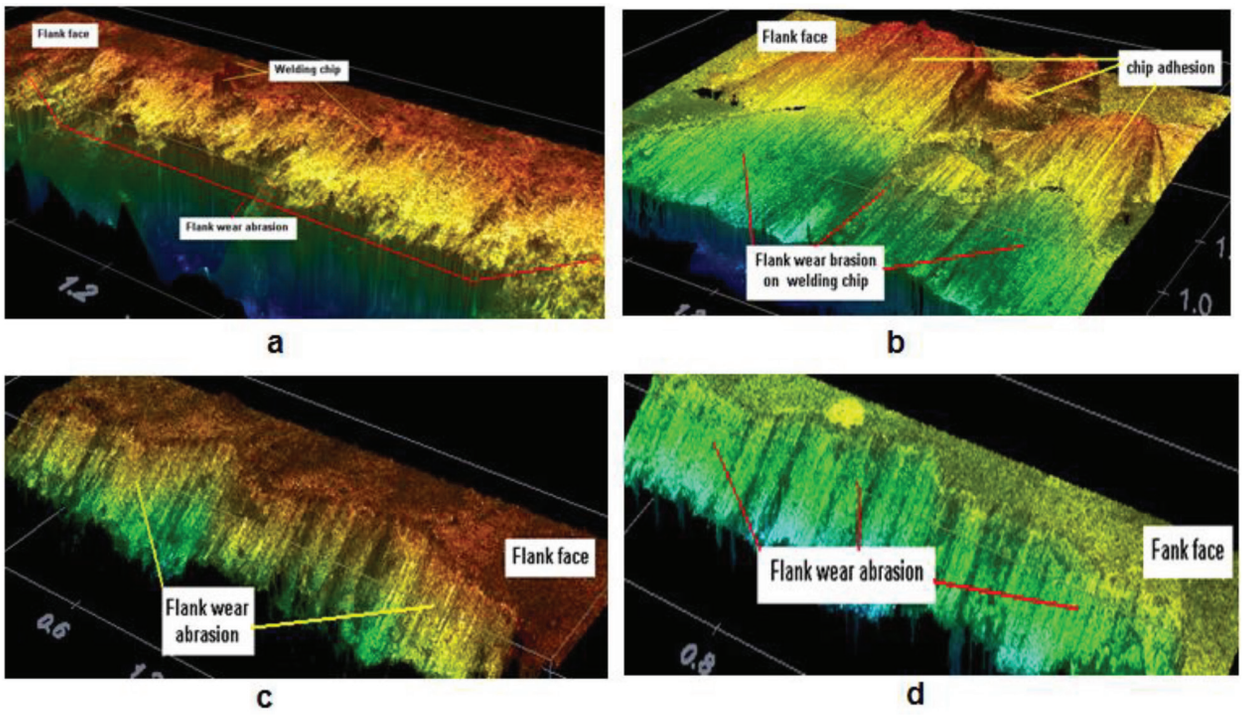

Figure 12. (a) 3D confocal image of the flank wear according (Vc = 600 m/min, f = 0.1 mm/rev, ap = 3 mm) for coating TiN insert. (b) Confocal image of the flank wear according (Vc = 800 m/min, f = 0.1 mm/rev, ap = 3 mm) for coating TiN insert. (c) 3D confocal image of the flank wear according (Vc = 1000 m/min, f = 0.1 mm/rev, ap = 3 mm) for coating TiN insert. (d) 3D confocal image of the flank wear according (Vc = 1200 m/min, f = 0.1 mm/rev, ap = 3 mm) for coating TiN insert.

Figure 13. Orthogonal cutting zone. Zone 1 Primary shearing zone. Zone 2 Secondary shearing zone (interface friction tool/chip). Zone 3 Tertiary friction (interface tool/workpiece zone).

flank wear caused by abrasion. **Figure 9c** shows a flank wear caused by high abrasion under (Vc = 1000 m /min, f = 0.1 mm/rev, ap = 3 mm), conditions.

C. Chip morphology investigation

First investigations concerning the chip morphology obtained in very high speed orthogonal turning by H13A uncoated and coated inserts tool material.

Using the optical microscope with high definition the Serrated chip obtained from experiments is showing in **Figure 13**.

Geometry of the chip shape in these experiments was systematically investigated at each cutting conditions using optical microscopy. The chips produced were collected and polished to

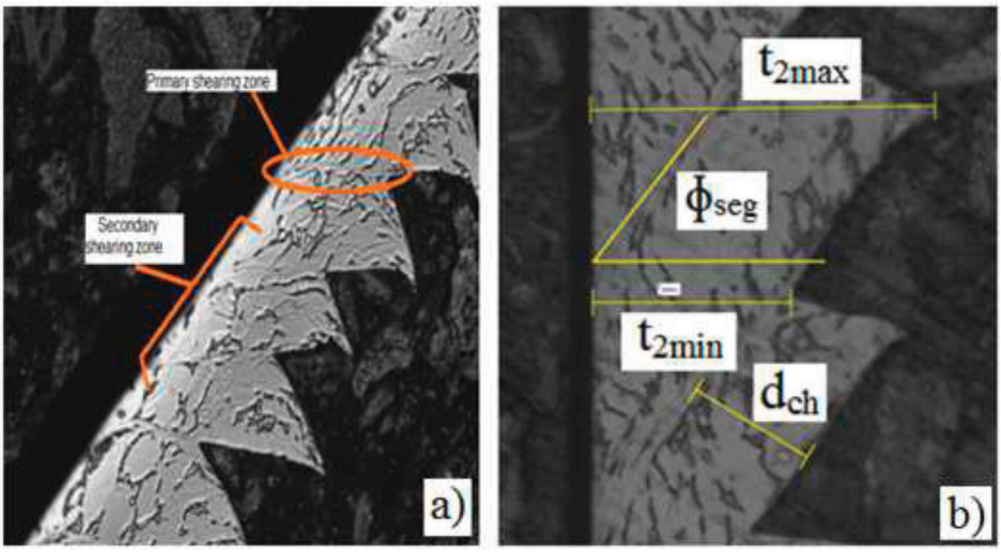

Figure 14. Serrated chip shape from experiments showing (a) shear zones, (b) the measured parameters [12].

measure the thicknesses t_{2max} and t_{2min}, d_{ch} the distance between each segments and ϕseg the inclination angle, see **Figure 14**. From t_{2max} and t_{2min} values, the degree of segmentation G was evaluated by:

$$G = \frac{t_{2max} - t_{2min}}{t_{2max}} \quad (1)$$

In high-speed machining the chip is segmented. The degree of segmentation gives an idea of the shear rate. This quantity indicates whether or not the chip is forming well and that the machining conditions are good.

Some pictures of serrated chips obtained for different cutting speeds, uncoated and coated TiN carbide inserts are presented in **Table 3** with 600 m/min cutting speed, and uncoated insert we see the chip is segmented, but it is not uniform. For the cutting speed 800 m/min, the chip is almost continuous, it is poorly segmented despite.

Significant strain in the shear zone. At the speed of 1000 m/min, the chip is uniform and well segmented, machining conditions are favorable a 1200 m/min, the chip is segmented at the beginning of machining, it is no longer uniform end machining (**Figure 15**).

As described in the introduction part, the shear angle ϕ and the inclination angle of a segment ϕ_{seg} are differentiated as shown in (**Figure 15**). The angle ϕ_{seg} is actually measured on the collected chips while the shear angle ϕ cannot be. The angle ϕ represents the initial shear similar to the one

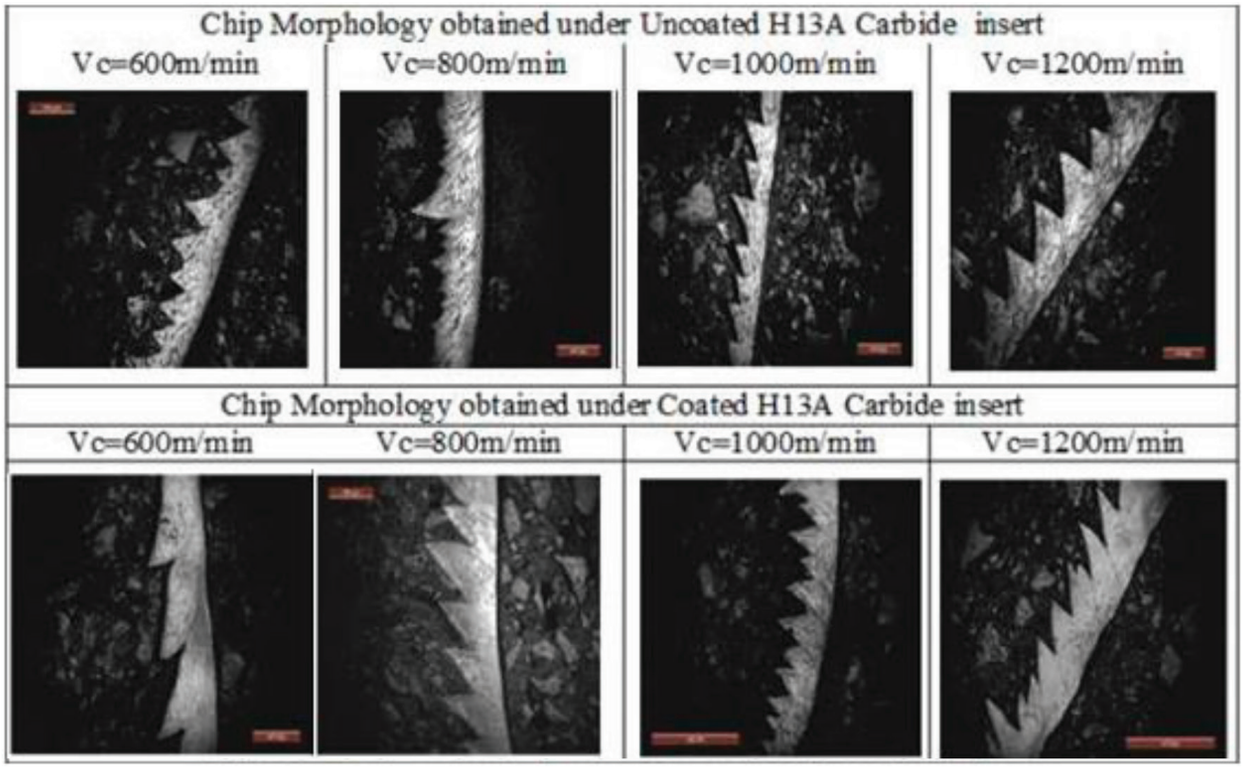

Table 3. Photography of chip morphology.

http://dx.doi.org/10.5772/intechopen.78669

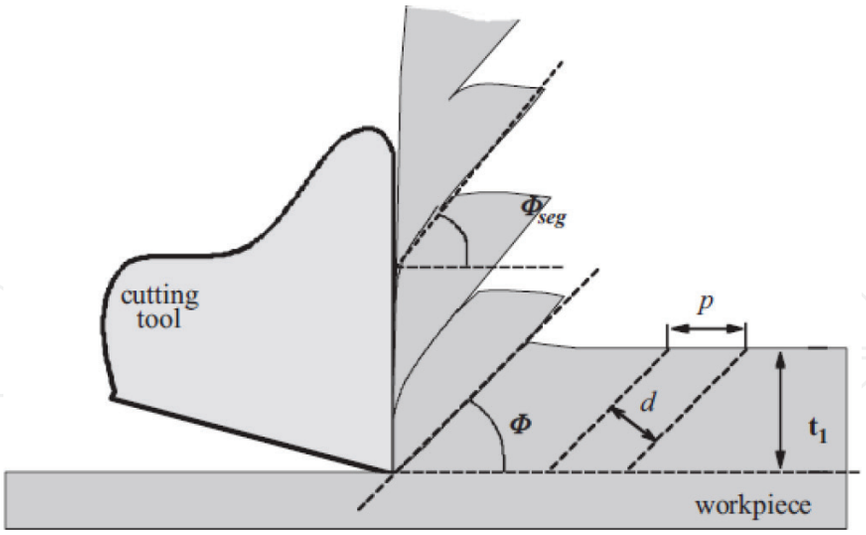

Figure 15. Schematic diagram of the serrated chip [12].

that describes the formation of a continuous chip in the primary shear zone. Considering that an element of volume, characterized by the angle ϕ, the length p and the width d is the source of a segment with the inclination ϕ_{seg} and the width d_{ch}, by applying the condition of incompressibility in plastic deformation, we obtain the balance equation Finally, with the assumption that the values of d and d_{ch} are close ($d = d_{ch}$), the initial shear angle f may be estimated by the following equation:

$$\varnothing = arc\ 0\sin\left(\frac{t_1}{(t_{2max}/\cos\varnothing\,seg) - d_{ch}\tan\varnothing\,seg}\right) \quad (2)$$

D. Analysis of the chip segmentation (Table 4)

Figure 16 shows that the degree of segmentation varies with the cutting speed. The largest value is recorded for the speed Vc = 1000 m/min. as speed increases, the degree of segmentation decreases. The variation of the degree of segmentation is more important for the TiN coated insert.

Figure 17 shows that the shear angle of the chip is larger for the coated insert. This value decreases substantially at 1000 m/min cutting speed and then increases towards 1200 m/min.

Cutting speed m/min								
	Uncoated	Coated	Uncoated	Coated	Uncoated	Coated	Uncoated	Coated
t_{2max}	0.298	0.231	0.320	0.209	0.139	0.384	0.302	0.222
t_{2min}	0.154	0.147	0.173	0.141	0.053	0.125	0.121	0.106
G	0.483	0.360	0.460	0.320	0.610	0.640	0.600	0.520
ϕseg	44°	73°	41°	37°	40°	59°	53°	59°
d_{ch}	0.111	0.088	0.111	0.078	0.056	0.181	0.112	0.070

Table 4. Parameters value of chip morphology.

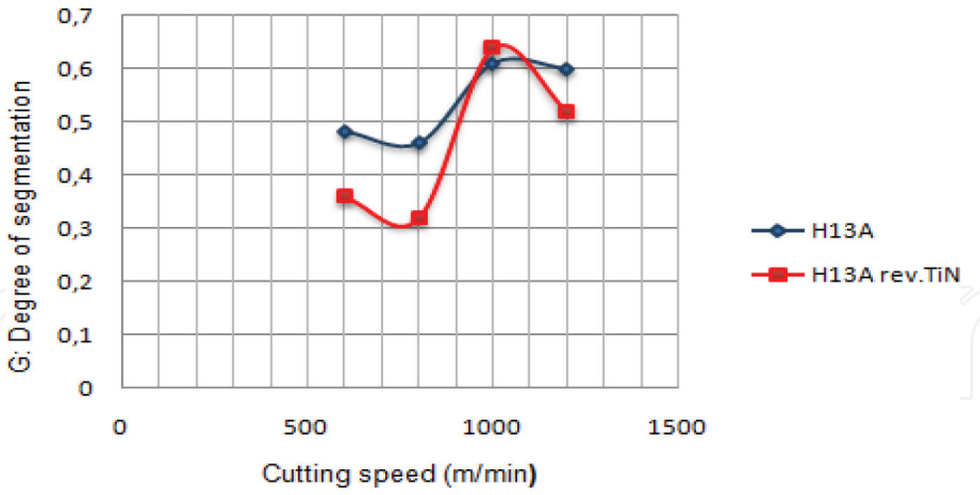

Figure 16. Degree of chip segmentation G evolution.

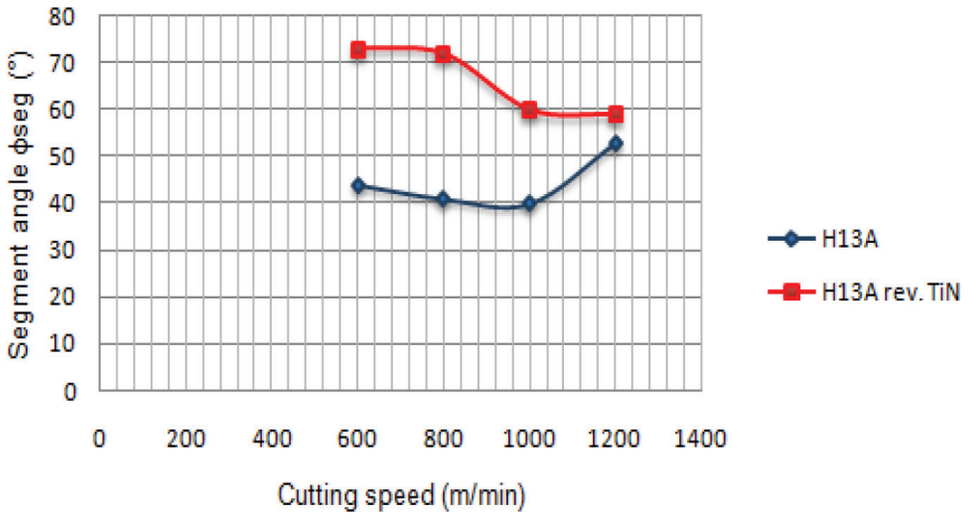

Figure 17. Evolution of shear angle ϕ.

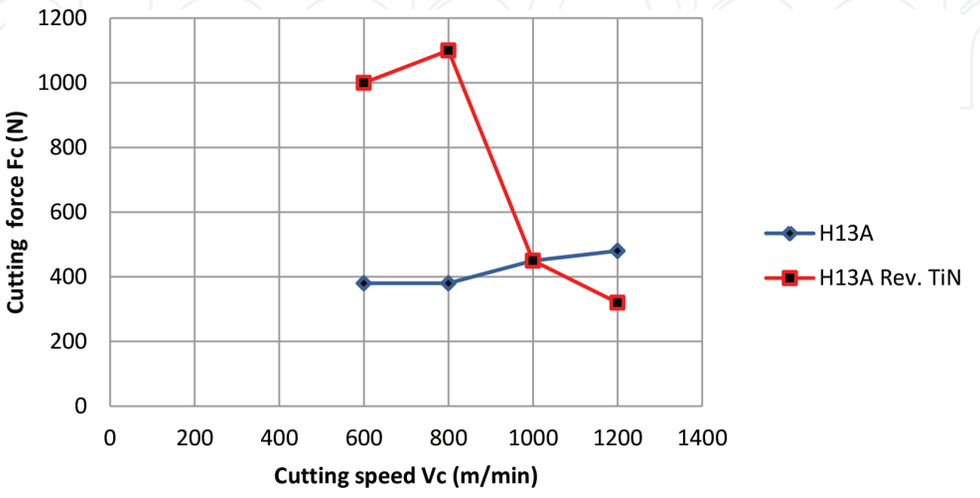

Figure 18. Cutting force evolution according cutting speed for uncoating and TiN coating inserts.

E. Cutting force evolution

The cutting forces measured at the beginning of the cut for each condition are given in **Figure 18**. Since the forces were measured at the beginning of the cut (first 5 s), it can be assumed that tool wear is negligible and therefore, the observed cutting forces are a function of the workpiece shear strength, chip shear angle and friction between the workpiece and tool.

Figure 18 shows the evolution of the cutting force Fc according to different cutting speeds. For H13A insert the cutting force Fc did not increase significantly. For TiN coated insert the cutting force Fc is important for cutting speeds (600 and 800 m/min), it greatly decreases in the speeds range (1000/1200 m/min). We explained this by the fact for the uncoated H13A plate there is no strong adhesion of the chip. For H13A coating TiN in cutting speed range (600/800 m/min). There was a strong adhesion of the chip with the cutting face which generates a large friction. The high cutting speed facilitates the removal of the chip and reduces adhesion. The cutting force is reduced.

4. Conclusion

Preliminary conclusion that can be given are:

At very high-speed machining of titanium alloy is possible. The detachment of the chip causes it to migrate carbide grains.

The goal of this work was to propose a detailed analysis of geometry of the chip alloy Ti–6Al–4 V.

The originality of this approach lies in the speed range explored varying between 600 and 1200 m/min that corresponds for carbide tools to the field of high speed (500 m/min) and very high speed (upper 600 m/min). This analysis helps to and proposes a hypothesis of their generation during high-speed machining. The ability to save snapshots of the cut in progress has complemented the postmortem micrographic analysis of chips and strengthens the hypotheses.

Almost instantaneous increase temperature in the cutting area of the chip causes the welding of the titanium alloy. The detachment of the chip causes it to migrate carbide grains.

In speed machining wear crater is the dominant wear on rake face and the final result is collapse in cutting edge.

Microgeometry analysis of cutting edges is very important in the understanding of the chip removal process. The interactions between the tool parameters, cutting parameters and the effects on the machining procedure are all influenced and therefore determined by the peak microgeometry. The evolution of the topography of crater wear using a confocal laser scanning microscopy is a valuable tool for crater imaging. It provides more details than conventional profilometers.

The chip formation of Ti-6Al-4 V alloy section is strongly influenced by crack initiation and propagation, resulting in discontinuous or fragmentary morphology. When machining Ti-6Al-4 V alloy at low cutting speed, the resulting chip is discontinuous, while at high cutting speed, chip is serrated.

Adhesion of the workpiece material occurs during titanium alloy machining, forming a BUE along the cutting edge. This BUE modifies the geometry of cutting edge and, consequently, the cutting forces. A better understanding of the relationship between cutting forces and both the shape and the size of the BUE must be realized in the future. It might be interesting to carry out tests with higher feed rates (by example 0.2 mm^{-1}). In terms of chip formation we notice adiabatic shear even at the lowest cutting speeds. This phenomenon is typical of titanium alloys.

To reduce wear, we must develop a system of lubrication located using the MQL technique.

Find a hard coating that will oppose the chip welding titanium alloy with the substrate of the insert. Why you should test other types of diamond coating for example.

Develop cryogenic lubrication to prevent heating in the cutting area.

Author details

Mohieddine Benghersallah[1]*, Lakhdar Boulanouar[1], Gautier List[2] and Guy Sutter[2]

*Address all correspondence to: bengher_moh@yahoo.fr

1 Research Laboratory in Advanced Technology and Mechanical Production, Department of Mechanical Engineering, Badji Mokhtar Annaba University, Annaba, Algeria

2 LEM3, UMR 7239, Université de Lorraine – Ile du Saulcy, Metz Cedex, France

References

[1] Boyer RR. An overview on the use of titanium in the aerospace industry. Materials Science and Engineering. 1996;**213A**:103-114

[2] Ezugwu EO, Wang ZM. Titanium alloys and their machinability, a review. Journal of Materials Processing Technology. 1997;**68**:262-274

[3] Nouari M, Makich H. Experimental investigation on the effect of the material microstructure on tool wear when machining hard titanium alloys: Ti–6Al–4V and Ti-555. International Journal of Refractory Metals and Hard Materials. 2013:259-269

[4] Ozel T, Ulutan D. Prediction of machining induced residual stresses in turning of titanium and nickel based alloys with experiments and finite element simulations. CIRP Annals-Manufacturing Technology. 2012;**61**:547-550

[5] Sutter G, List G. Very high speed cutting of Ti–6Al–4V titanium alloy – Change in morphology and mechanism of chip formation. International Journal of Machine Tools & Manufacture. 2013;**66**:37-43

[6] Nouari M, Calamaz M, Girot F. Mécanismes d'usure des outils coupants en usinage à sec de l'alliage de titane aéronautique Ti–6Al–4V. Comptes Rendus Mecanique. 2008;**336**: 772-781

[7] Olortegui-Yume JA, Kwon PY. Crater wear evolution in multilayer coated carbides during machining using confocal microscopy. Journal of Manufacturing Processes. 2007;**9**(1):107-110

[8] Liu Z, An Q, Xu J, Han MCS. Wear performance of (AlTiN)/(Si3N4) coating and (AlCrN)/(Si3N4) coating in high-speed machining of titanium alloys under dry and minimum quantity lubrication (MQL) conditions. Wear. 2013;**305**:249-259

[9] Zuo JH, Wang ZG, Han EH. Effect of microstructure on ultra-high cycle fatigue behavior of Ti–6Al–4V. Master Science Engineering A. 2008;**473**:147-152

[10] Sharman ARC, Aspinwall DK, Dewes RC, Bowen P. Work piece surface integrity considerations when finish turning gamma titanium aluminide. Wear. 2001;**249**:473

[11] Niu W, Berminghama MJ, Baburamani PS, Palanisamy S, Dargusch MS, Turk S, Grigson B, Sharp PK. The effect of cutting speed and heat treatment on the fatigue life of Grade 5 and Grade 23Ti–6Al–4V alloys. Materials & Design; April 2013;**46**:640-644

[12] Sharif S, Rahim EA. Performance of coated- and uncoated-carbide tools when drilling titanium alloy—Ti– 6Al4V. Journal of Materials Processing Technology. 2007;**185**:72-76

[13] Mathia T, Zahouani H, Rousseau J, Le Bosse JC. Functional significance of different techniques for surface morphology measurements. International Journal of Machine Tools and Manufacture. 1995;**35**:195-202

[14] Corle T, Kino G. Confocal Scanning Optical Microscopy and Related Imaging Systems. San Diego: Academic Press; 1996

[15] Bennett JM. Overview: Sensitive techniques for surface measurement and characterization. In: Proceedings of SPIE 1573. 1991. pp. 152-158

[16] Hamilton DK, Wilson T. Surface profile measurement using the confocal microscope. Journal of Applied Physics. 1982;**53**:5320-5322

[17] Devillez A, Lesko S, Mozer W. Cutting tool crater wear measurement with white light interferometry. Wear. 2004;**256**:56-65

[18] Dawson TG, Kurfess TR. Quantification of tool wear using white light interferometry and three-dimensional computational metrology. International Journal of Machine Tools and Manufacture. 2005;**45**:591-596

[19] HK T, Denkena B. Basics of Cutting and Abrasive Processes. Berlin: Springer; 2013

[20] Lichtman J. la microscopie confocale pour la science. octobre 1994. p. 204

[21] Zhu D, Xiaoming Z, Ding H. Tool wear characteristics in machining of nickel-based superalloys. International Journal of Machine Tools & Manufacture. 2013;**64**:60-77

[22] Sun S, Brandt M, Dargusch MS. Characteristics of cutting forces and chip formation in machining of titanium alloys. International Journal of Machine Tools & Manufacture. 2009;**49**:561-568

[23] Mathia TG, Pawlusb P, Wieczorowskic M. Recent trends in surface metrology. Wear. 2011;**271**:494-508

[24] Bassett E, Köhler J, Denkena B. On the honed cutting edge and its side effects during orthogonal turning operations of AISI1045 with coated WC-co inserts. CIRP Journal of Manufacturing Science and Technology. 2012;**5**:108-126

[25] Winogrodzka A, Valefi M, de Rooij MB, Schipper DJ. Measurement of chemical and geometrical surface changes in a wear track by a confocal height sensor and confocal Raman spectroscopy. Archives of Civil And Mechanical Engineering. 2014;**14**:1-5

[26] Denkena B, Biermann D. Cutting edge geometries. CIRP Annals-Manufacturing Technology. 2014;**63**:631-653

[27] Al-Zkeri I, Rech J, Altan T, Hamdi H, Valiorgue F. Optimization of the cutting edge geometry of coated carbide tools in dry turning of steels using a finite element analysis. Machining Science and Technology. 2009;**13**(1):36-51

[28] Revue sandvik coromant. Trametal-Janvier/Fevrier. 2010. p. 134

[29] Wong T, Kim W, Know P. Experimental support for a model-based prediction of tool wear. Wear. October 2004;**257**(7-8):790-798

[30] Olortegui-Yume JA, Kwon PY. Tool wear mechanisms in machining. International Journal of Machining and Machinability of Materials. 2007. Inderscience